NAVIER-STOKES-BASED REGULARIZATION FOR 4D FLOW MRI SUPER-RESOLUTION

Sébastien Levilly, Saïd Moussaoui, Jean-Michel Serfaty

NAVIER-STOKES-BASED REGULARIZATION FOR 4D FLOW MRI SUPER-RESOLUTION

Sébastien LEVILLY[⋆†] *Saïd MOUSSAOUI*[†] *Jean-Michel SERFATY*[⋆]

[⋆] Nantes Université, CHU Nantes, CNRS, INSERM, Institut du thorax, Nantes, France
[†] Nantes Université, École Centrale Nantes, CNRS, LS2N, Nantes, France

ABSTRACT

4D flow MRI is a promising tool in cardiovascular imaging. However, its lack of resolution can degrade some biomarkers' evaluation accuracy. The computational fluid dynamics (CFD) simulation is considered as the reference method to improve numerically the image resolution. However, CFD simulations are complex and time consuming, and matching their results with 4D Flow MRI data is very challenging. This paper aims to introduce a fast and efficient super-resolution (SR) approach thanks to the minimization of a L_2-penalized criterion, which combines a weighted least-squares data fidelity term and Navier-Stokes equations. The algorithm has been validated on synthetic and phantom datasets and compared to state-of-the-art solutions. Moreover, a prospective study is conducted on the segmentation-free application of the proposed algorithm.

***Index Terms*—** 4D Flow MRI, super-resolution, CFD, inverse problems, segmentation-free

1. INTRODUCTION

Nowadays in clinical routine for cardiovascular diagnosis, flow imaging is mostly limited to 2D Phase-Contrast MRI. Over the last five years however, 4D Flow MRI [1] has become an interesting tool for clinicians, due to its ability to measure the anatomy and the three velocity components within a 3D volume and along the cardiac cycle. The image reconstruction is applied on a regular spatio-temporal grid whose resolution is known to be limited [1, 2] due to the trade-off between resolution, signal-to-noise ratio and acquisition time. Therefore, accurate quantification of biomarkers from such data becomes challenging. Indeed, the lack of resolution has a direct impact on the computation of spatial derivatives which are involved in the evaluation of biomarkers such as the wall shear stress [3, 4]. Besides, this lack of resolution can have an additional effect through a coarse wall definition. Consequently, the evaluation of every biomarker depending on the velocity field can be improved by enhancing the 4D flow image resolution.

The computational fluid dynamics (CFD) simulation is the reference solution to improve the velocity field resolution and get biomarkers with velocities fulfilling fluid mechanical laws [5]. However, CFD simulations are based on non-linear equations named Navier-Stokes, whose numerical resolution requires a precise estimation of the fluid domain and the inlet/outlet velocity fields (or by default the mass flow rate). To improve the CFD simulation and the data matching process, previous contributions were inspired from computer vision [6, 7], machine learning [8, 9] and inverse problem theory [10, 11, 12, 13]. In the latter category, some data assimilation approaches enforce the Navier-Stokes equations as a hard constraint which leads to run several CFD simulations with an iteratively updated inflow [11, 12]. Rispoli *et al.* [10] algorithm is inspired from a CFD solver called SIMPLER [14] which avoids the repetition of CFD simulations. However, the divergence-free equation implies the solving of a Poisson equation to get the pressure and this step significantly slowdown the algorithm performance. Besides, most previous strategies [10, 11, 12, 13] use a pre-established fluid domain segmentation which entails a time consuming step before the super-resolution (SR) application. Both imposing the Navier-Stokes equations and using a pre-established segmentation weaken the SR interest.

This paper aims to introduce a fast and efficient SR approach, based on inverse problem theory [15], in which the segmentation knowledge is not mandatory. The proposed solution is based on a L_2-penalized formulation to improve the computation time. The criterion, detailed in section 2, is made of two terms: a weighted data fidelity one and a penalization one using Navier-Stokes equations. Akin to previous contributions [10, 11, 13], the downsampling model of the acquisition process is used to reconstruct velocities on a thinner grid. Moreover, we propose to introduce a spatial weighting of the data fitting term, based on the *a priori* standard deviation [2]. Such scheme can be viewed as a soft-segmentation. Moreover, the Navier-Stokes equations are accounted for in a penalization approach rather than a hard constraint so as to reduce the computation time. The linearization of the Navier-Stokes equations is performed using the finite-volume method [10, 16]. For the sake of simplicity, this study is led on 2D sections of simulated synthetic data and experimental 4D flow MRI measurements on a phantom (see section 3). In section 4, results are evaluated in terms of root-mean-square error of the velocity vector in the fluid domain and the computation time. Finally, a prospective analysis is conducted on

the opportunity to perform the SR without a pre-established segmentation.

2. METHODS

Let's define the data velocity vector $\mathcal{Y} = (\boldsymbol{u}_{\mathrm{d}}^{\mathrm{t}}, \boldsymbol{v}_{\mathrm{d}}^{\mathrm{t}}, \boldsymbol{w}_{\mathrm{d}}^{\mathrm{t}})^{\mathrm{t}}$ where $\boldsymbol{u}_{\mathrm{d}}$, $\boldsymbol{v}_{\mathrm{d}}$ and $\boldsymbol{w}_{\mathrm{d}}$ are stacked in the lexicographic order. The unknown vector is denoted by $\mathcal{X} = (\boldsymbol{u}^{\mathrm{t}}, \boldsymbol{v}^{\mathrm{t}}, \boldsymbol{w}^{\mathrm{t}}, \boldsymbol{p}^{\mathrm{t}})^{\mathrm{t}}$ where $\boldsymbol{u}$, $\boldsymbol{v}$ and $\boldsymbol{w}$ are the estimated velocities over the super-resolved grid and $\boldsymbol{p}$ is the estimated pressure field. In order to improve numerically the spatial resolution, we propose to solve the following non-linear optimization problem:

$$\hat{\mathcal{X}} = \underset{\mathcal{X} \in \mathrm{R}^N}{\arg\min} \, \|\mathcal{Y} - \mathbf{H}\mathcal{X}\|_{\mathbf{W}}^2 + \lambda \mathcal{NS}(\mathcal{X}) \tag{1}$$

where N is the unknown vector size, $\mathbf{H}$ represents the acquisition sampling process, $\mathbf{W}$ is a diagonal weight matrix of *a priori* velocity variances, and $\mathcal{NS}$ is a regularization term based on the Navier-Stokes equations and weighted by λ.

Akin to previous contributions [10, 11, 13], a 4D flow MRI point spread function (PSF) is used to link super-resolved velocities with the measured ones. For the sake of simplicity, a mean filter was used to model the downsampling process, leading to averaged super-resolved velocity components within each data voxel. However, more sophisticated models can be introduced to include the 4D flow MRI PSF [10]. Besides, the measured velocity is obtained from the MRI phase contrast and consequently have a spatially variant standard deviation [2] such as:

$$\sigma_{\mathrm{v},i} = \frac{\sqrt{2}}{\pi} \frac{V_{\mathrm{enc}}}{\mathrm{SNR}_i} \tag{2}$$

where V_{enc} is the encoding velocity, and SNR_i the signal-to-noise ratio of the anatomical signal in the i-th voxel. In the proposed solution, the weight matrix is defined by $\mathbf{W} = \mathrm{diag}\{\frac{1}{2\sigma_{\mathrm{v},i}^2}\}_{i=1\ldots N_{\mathrm{d}}}$ in order to reduce the weight of velocities outside regions of interest and potentially guide a segmentation-free solving.

Since blood density ρ and dynamic viscosity μ are assumed to be constant, the velocity $\vec{v} = (u, v, w)^{\mathrm{t}}$ is governed by the incompressible Navier-Stokes equations with the mass conservation equation and the momentum conservation equations:

$$\mathrm{div}(\vec{v}) = 0 \tag{3}$$

$$\rho \, \overline{\overline{\mathrm{grad}}}(\vec{v}) \cdot \vec{v} - \mu \, \Delta \vec{v} + \overline{\mathrm{grad}} \, p = \vec{0} \tag{4}$$

where p is the pressure. In our application, body forces and the transient velocity terms are assumed to be negligible. Dirichlet conditions were applied on every border with a no-slip condition on the wall and interpolated data velocity on the inlet and outlet. A common strategy to get a first order approximation of these equations is to use the finite-volume method, which relies on equations (3) and (4) integration over the voxels' volume [14, 10, 16]. Consequently, equations (3) and (4) can be linearized at any point $\mathcal{X}_k$, leading to a quadratic regularization term $\mathcal{NS}_k$:

$$\mathcal{NS}_k(\mathcal{X}) = \|\mathbf{S}_{\mathcal{X}_k}\mathcal{X} - \boldsymbol{b}\|_2^2 \tag{5}$$

where $\mathbf{S}_{\mathcal{X}_k}$ is the convection-diffusion matrix computed from $\mathcal{X}_k$ and $\boldsymbol{b}$ contains the boundary conditions either on the field-of-view or on the pre-established segmentation borders. Contrary to the proposed approach in Rispoli *et al.* [10], all the velocity components are updated simultaneously by using a coupled velocity-pressure formulation [16]. In that respect, an iterative scheme is proposed to solve the non-linear problem (1) by defining the weighted least-squares criterion for each $\mathcal{X}_k$:

$$\min_{\mathcal{X} \in \mathrm{R}^N} \|\mathcal{Y} - \mathbf{H}\mathcal{X}\|_{\mathbf{W}}^2 + \lambda \|\mathbf{S}_{\mathcal{X}_k}\mathcal{X} - \boldsymbol{b}\|_2^2 \tag{6}$$

whose solution $\hat{\mathcal{X}}$ is obtained by solving the following linear system:

$$\left(\mathbf{H}^{\mathrm{t}}\mathbf{W}\mathbf{H} + \lambda \, \mathbf{S}_{\mathcal{X}_k}^{\mathrm{t}}\mathbf{S}_{\mathcal{X}_k}\right)\mathcal{X} = \left(\mathbf{H}^{\mathrm{t}}\mathbf{W}\mathcal{Y} + \lambda \, \mathbf{S}_{\mathcal{X}_k}^{\mathrm{t}}\boldsymbol{b}\right) \tag{7}$$

using a linear biconjugate gradient stabilized algorithm. The efficiency of this iterative scheme comes also from the reduction of memory usage and computational load by using operators for $\mathbf{H}$, $\mathbf{S}_{\mathcal{X}_k}$ and $\mathbf{W}$ instead of constructing large sparse matrices. The resolution algorithm convergence is checked once the normalized residual between two iterations, $\|\hat{\mathcal{X}}_k - \hat{\mathcal{X}}_{k-1}\|_2^2 / \|\hat{\mathcal{X}}_{k-1}\|_2^2$, is below the tolerance threshold (10^{-6}).

3. VALIDATION

The proposed Penalized-SR (PSR) approach has been validated on 2D sections of simulated synthetic data and experimental 4D flow MRI measurements, which are presented in Fig.1. First, the fluid domain of the synthetic data is a straight tilted cylinder, with a radius of 1.5 cm, and within a larger rectangular field-of-view of 15×8.63 cm^2. Since we consider a non-pulsatile flow, it is governed by the Poiseuille model, a quadratic flow with a maximum velocity of 0.75 m/s. The dynamic viscosity μ and fluid density ρ are set to 0.0032 Pa.s and 1060 Kg/m^3. To simulate 4D flow MRI, the Poiseuille flow is evaluated on a thin grid with an isotropic (ISO) spatial resolution of 1 mm. Then, a mean filter is applied to the high resolution velocity grid to account for the downsampling process. Finally, the zero-mean Gaussian noise added to the filtered velocity field is spatially variant using the *a priori* standard deviation $\sigma_{\mathrm{v},}$. A noise standard deviation of $5\,\%$ of V_{enc} is ensured within the fluid domain while the resulting velocity outside is limited by V_{enc}. Besides, the encoding velocity V_{enc} is set to $120\,\%$ of the maximum velocity.

The phantom 4D flow MRI data were retrieved from the contribution of Castagna *et al.* [17]. This experimental setup is composed of a straight square pipe with a section $25 \times$

$25\ \mathrm{mm}^2$, a MRI-compatible gear pump (CardioFlow 5000, Shelley Medical Technology) and a reservoir. Here, we only consider 4D flow MRI data with a steady flow of $98.7\ \mathrm{mL/s}$ and a maximal velocity of $28\ \mathrm{cm/s}$. The 4D flow MRI spatial resolution is $2.2 \times 2.2 \times 2\ \mathrm{mm}^3$ while the studied 2D section has a pixel-size of $2.2 \times 2.2\ \mathrm{mm}^2$. The reference flow of this dataset comes from a CFD simulation using finite-volume method (Star CCM+, Siemens) on a Cartesian mesh of $1{,}725{,}000$ $0.5\ \mathrm{mm}$-size cubic elements.

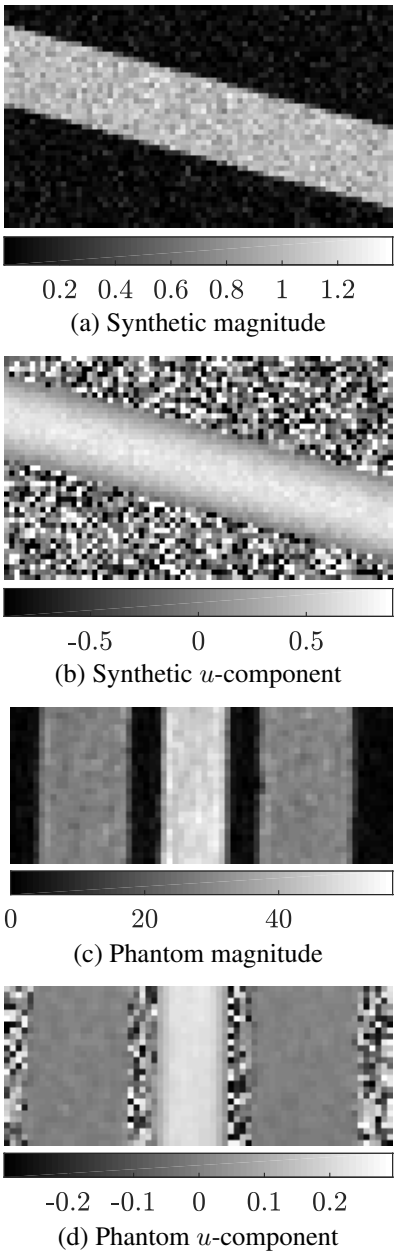

(a) Synthetic magnitude

(b) Synthetic u-component

(c) Phantom magnitude

(d) Phantom u-component

Fig. 1. Synthetic and Phantom datasets (velocity in $\mathrm{m/s}$).

Both these datasets are analyzed in terms of Root-Mean-Square Error (RMSE) of the super-resolved estimation within the fluid domain compared to their theoretical and numerical reference. The RMSE is defined as the percentage of the initial noise level in the residual such as:

$$\mathrm{RMSE}(\boldsymbol{r}) = {}^{1}\!/_{\mathrm{RMSE_d}} \times \sqrt{{}^{\Sigma_{i=1}^{N}(\boldsymbol{r}_i-\bar{\boldsymbol{r}}_i)^2}\!/_{N}} \qquad (8)$$

where $\bar{\boldsymbol{r}}$ is the super-resolved reference velocity field, $\mathrm{RMSE_d}$ is equal to $\sqrt{\frac{1}{N_\mathrm{d}} \sum_{i=1}^{N_\mathrm{d}} \left(\mathcal{Y}_i - \bar{\mathcal{Y}}_i\right)^2}$ with N_d the size of $\mathcal{Y}$, and the vector $\bar{\mathcal{Y}}$ containing the low resolution reference velocity field. Finally, the proposed PSR, and Rispoli *et al.* [10], named SbSR for SIMPLER based-SR, solutions are then compared in terms of RMSE and computation time. Penalization parameters λ of SbSR and PSR were optimized by minimizing RMSE on each dataset.

4. RESULTS & DISCUSSION

Both PSR and SbSR solutions were evaluated on the datasets in Fig.1 under the constraint of the fluid location knowledge. For the sake of simplicity, Fig.2 shows the super-resolution of only the u-component of the velocity. The two upper images of Fig.2 display both algorithm reconstructions on synthetic data while the two lower ones demonstrate the super-resolution effectiveness on phantom data. One can observe nonzero values on the inlet and outlet which are due to the significant weight λ given to the Navier-Stokes equations (between 10^5 and 10^8) and the data input on these borders (added in the vector $\boldsymbol{b}$).

Regarding the RMSE performance, SbSR successfully improves the resolution of the synthetic dataset by a factor 2×2 with a residual RMSE of $59.9\,\%$ while our PSR approach reaches a residual RMSE of $30.3\,\%$. A similar results is observed on the phantom dataset with a RMSE of $89.2\,\%$ for SbSR and $39.2\,\%$ with the PSR solution. Thus, the proposed solution contains only half residual error compared to SbSR, and reduces $60-70\,\%$ of the initial error. As the noise standard deviation is set to $5\,\%$ of V_{enc}, the resulting error is smaller than $2\,\%$ of V_{enc}. These results demonstrate the interest of a fully penalized solution in comparison with the divergence-free constraining in SbSR.

These calculations were realized with MATLAB (R2020b) on a workstation with an Intel Core i7-6820HQ (2.70GHz) and 32Gb of RAM. On the synthetic dataset, 489 seconds are necessary to converge with SbSR while it is only 14 seconds for the PSR. For the phantom dataset, the SbSR and PSR solution have converged after 181 seconds and 7 seconds respectively. Most of the computation time difference is due to the divergence-free constraint with a Poisson equation solving which hamper the SbSR computational performance. In that context, PSR solution performances stem from the formulation of a penalized criterion, since Navier-Stokes linearization and optimized operators were employed for both SR algorithms.

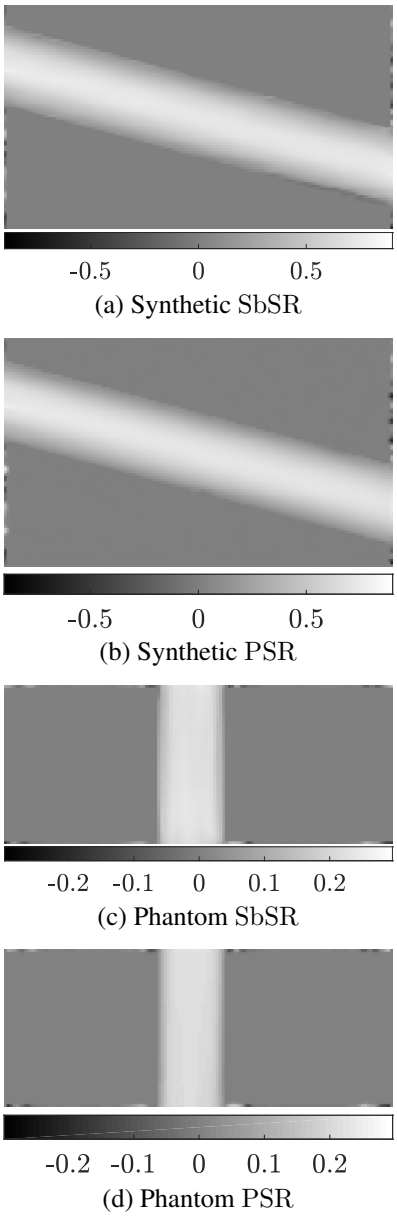

(a) Synthetic SbSR
(b) Synthetic PSR
(c) Phantom SbSR
(d) Phantom PSR

Fig. 2. Super-resolved velocity field $[\mathrm{m/s}]$.

Finally, an analysis on the opportunity to not use any segmentation was carried out with PSR and presented in Fig.3. SbSR algorithm is not considered at this stage since it relies on a precise segmentation and would not converge due to high velocity fluctuation outside the lumen. As expected for PSR, the velocities outside the fluid domain are nonzero which leads to a serious RMSE degradation. Moreover, multiple computations of PSR led to RMSE fluctuations comprised in the intervals $44.2-55.9\,\%$ and $72.6-93.3\,\%$ for the synthetic and phantom datasets. Respectively, the computation time is also impacted with 813 and 482 seconds for the synthetic and phantom datasets. Actually, the data weight matrix $\mathbf{W}$ acts as

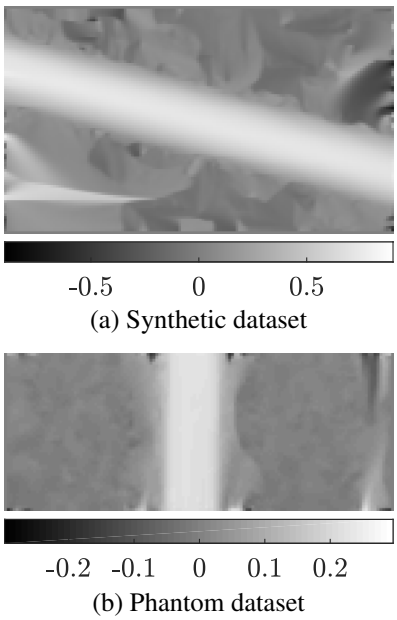

(a) Synthetic dataset
(b) Phantom dataset

Fig. 3. Segmentation-free super-resolved velocity field $[\mathrm{m/s}]$.

an implicit soft-segmentation which performs mainly within the fluid domain. Outer velocities are mostly affected by the Navier-Stokes equations whose inlet/outlet definition is partially erroneous. Although the RMSE is computed within the fluid area, the outer velocity estimation deteriorates actively the inner ones and particularly those close to the vessel wall.

One can prevent the PSR performance degradation by using a coarse dilated segmentation. The outer velocities close to the wall would change progressively and remain small since the segmentation enforce the no-slip condition. Another solution to conserve a segmentation-free strategy would be to regularize outer velocities using additional penalization criteria.

5. CONCLUSION

In this paper, a fast and efficient super-resolution solution is introduced. Based on inverse problem theory, it employs the Navier-Stokes equations as an additional prior information for the problem solving. These equations were used in a penalized formulation which allows faster resolution, in opposition to a constrained one, and still provides satisfying RMSE results. Furthermore, the segmentation knowledge is not mandatory to use the proposed solution. Future investigations will be conducted to fully benefit from an efficient segmentation-free solution. Additional prior information, for instance temporal, could be used to regularize outer velocities. Besides, pulsatile and clinical applications will be considered to observe more realistic blood flow patterns.

6. COMPLIANCE WITH ETHICAL STANDARDS

This is a numerical simulation and phantom study for which no ethical approval was required.

7. CONFLICTS OF INTEREST

The first author is employed by the University Hospital Center of Nantes and funded by the GIE grant from Philips company.

8. REFERENCES

[1] M. Markl, A. Frydrychowicz, S. Kozerke, M. Hope, and O. Wieben, "4D Flow MRI," *J. Magn. Reson. Imaging*, vol. 36, no. 5, pp. 1015–1036, 2012.

[2] N. J. Pelc, M. A. Bernstein, A. Shimakawa, and G. H. Glover, "Encoding strategies for three-direction phase-contrast MR imaging of flow," *J. Magn. Reson. Imaging*, vol. 1, no. 4, pp. 405–413, 1991.

[3] A. F. Stalder, M. F. Russe, A. Frydrychowicz, J. Bock, J. Hennig, and M. Markl, "Quantitative 2D and 3D phase contrast MRI: Optimized analysis of blood flow and vessel wall parameters," *Mag. Reson. Med.*, vol. 60, no. 5, pp. 1218–1231, 2008.

[4] S. Levilly, M. Castagna, J. Idier, F. Bonnefoy, D. Le Touzé, S. Moussaoui, P. Paul-Gilloteaux, and J.-M. Serfaty, "Towards quantitative evaluation of wall shear stress from 4D flow imaging," *Magn. Reson. Imaging*, vol. 74, pp. 232–243, 2020.

[5] L. Boussel, V. L. Rayz, A. Martin, G. Acevedo-Bolton, M. T. Lawton, R. Higashida, W. S. Smith, W. L. Young, and D. Saloner, "Phase-contrast magnetic resonance imaging measurements in intracranial aneurysms in vivo of flow patterns, velocity fields, and wall shear stress: comparison with computational fluid dynamics.," *Mag. Reson. Med.*, vol. 61, pp. 409–417, 02 2009.

[6] N. de Hoon, R. van Pelt, A. Jalba, and A. Vilanova, "4D MRI flow coupled to physics-based fluid simulation for blood-flow visualization," *Comput. Graph. Forum*, vol. 33, no. 3, pp. 121–130, 2014.

[7] F. M. Callaghan and S. M. Grieve, "Spatial resolution and velocity field improvement of 4D-flow MRI," *Mag. Reson. Med.*, vol. 78, no. 5, pp. 1959–1968, 2017.

[8] F. Gaidzik, D. Stucht, C. Roloff, O. Speck, D. Thévenin, and G. Janiga, "Transient flow prediction in an idealized aneurysm geometry using data assimilation," *Comput. Biol. Med.*, vol. 115, 2019.

[9] I. Perez-Raya, M. F. Fathi, A. Baghaie, R. H. Sacho, K. M. Koch, and R. M. D'Souza, "Towards multi-modal data fusion for super-resolution and denoising of 4D-flow MRI," *Int. J. Numer. Meth. Bio.*, vol. 36, no. 9, 2020.

[10] V. C. Rispoli, J. F. Nielsen, K. S. Nayak, and J. LA Carvalho, "Computational fluid dynamics simulations of blood flow regularized by 3D phase contrast MRI," *Biomed. Eng. Online*, vol. 14, no. 1, pp. 110, 2015.

[11] M. D'Elia, M. Perego, and A. Veneziani, "A variational data assimilation procedure for the incompressible Navier-Stokes equations in hemodynamics," *J. Sci. Comput.*, vol. 52, no. 2, pp. 340–359, 2012.

[12] S. W. Funke, M. Nordaas, Ø. Evju, M. S. Alnæs, and K. A. Mardal, "Variational data assimilation for transient blood flow simulations: Cerebral aneurysms as an illustrative example," *Int. J. Numer. Meth. Bio.*, vol. 35, no. 1, 2019.

[13] M. F. Fathi, I. Perez-Raya, A. Baghaie, P. Berg, G. Janiga, A. Arzani, and R. M. D'Souza, "Super-resolution and denoising of 4D-flow MRI using physics-informed deep neural nets," *Comput. Meth. Prog. Bio.*, p. 105729, 2020.

[14] S. V. Patankar, *Numerical Heat Transfer and Fluid Flow*, Series on Computational Methods in Mechanics and Thermal Science. Hemisphere Publishing Corporation (CRC Press, Taylor & Francis Group), 1980.

[15] J. Idier, *Bayesian Approach to Inverse Problems*, ISTE Ltd and John Wiley & Sons Inc, Apr. 2008.

[16] Z. Mazhar, *Fully Implicit, Coupled Procedures in Computational Fluid Dynamics*, vol. 115, Springer, Cham, 2016.

[17] M. Castagna, S. Levilly, P. Paul-Gilloteaux, S. Moussaoui, J. Rousset, F. Bonnefoy, J. Idier, J. Serfaty, and D. Le Touzé, "An LDV based method to quantify the error of PC-MRI derived wall shear stress measurement," *Sci. Rep.*, vol. 11, 2021.